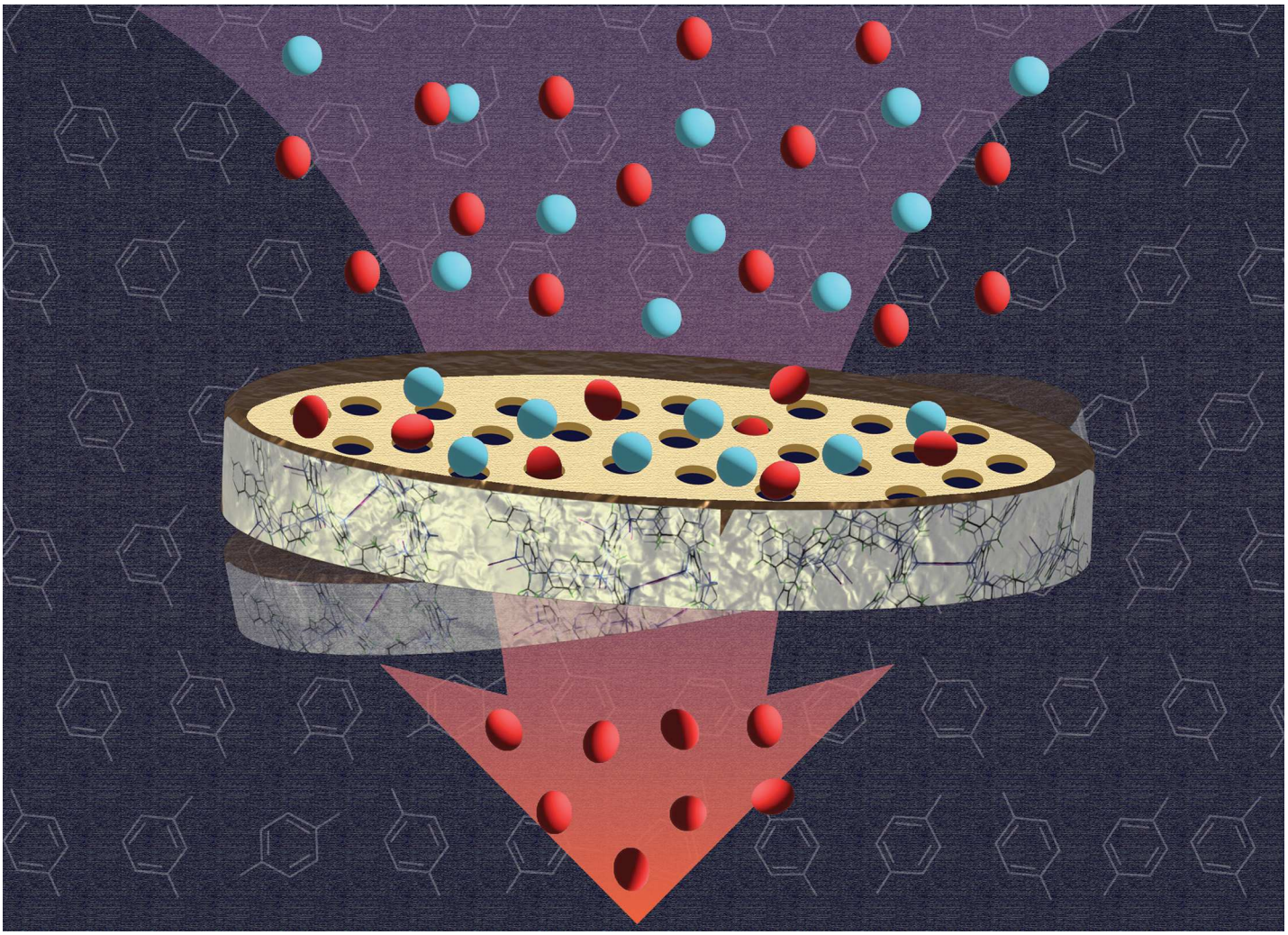

Showcasing research from Professor Ryan Lively's laboratory, School of Chemical & Biomolecular Engineering, Georgia Institute of Technology, Atlanta, Georgia, USA.

Unblocking a rigid purine MOF for kinetic separation of xylenes

Zn(purine)I showed excellent *para*-xylene/*ortho*-xylene separation capability with a diffusion selectivity of 6 and high equilibrium adsorption selectivity as indicated by coadsorption experiments. This is attributed to the shape and size of the channel aperture within the rigid framework of Zn(purine)I.

As featured in:

See Ryan P. Lively *et al.*, *Chem. Commun.*, 2022, **58**, 12305.

ROYAL SOCIETY OF CHEMISTRY

rsc.li/chemcomm

Registered charity number: 207890

ChemComm

COMMUNICATION

View Article Online
View Journal | View Issue

Cite this: *Chem. Commun.*, 2022, **58**, 12305

Received 8th August 2022,
Accepted 30th September 2022

DOI: 10.1039/d2cc04387d

rsc.li/chemcomm

Unblocking a rigid purine MOF for kinetic separation of xylenes†

Richelle Lyndon,‡[a] Yuxiang Wang, ‡[a] Ian M. Walton,[a] Yao Ma,[a] Yang Liu,[a] Zhenzi Yu,[a] Guanghui Zhu, [a] Samuel Berens,[b] Yu-Sheng Chen,[c] SuYin G. Wang,[c] Sergey Vasenkov, [b] David S. Sholl,[ad] Krista S. Walton, [a] Simon H. Pang [e] and Ryan P. Lively *[a]

The separation of xylene isomers still remains an industrially challenging task. Here, porous purine-based metal–organic frameworks (MOFs) have been synthesized and studied for their potential in xylene separations. In particular, Zn(purine)I showed excellent *para*-xylene/*ortho*-xylene separation capability with a diffusion selectivity of 6 and high equilibrium adsorption selectivity as indicated by coadsorption experiments. This high selectivity is attributed to the shape and size of the channel aperture within the rigid framework of Zn(purine)I.

Industrially, xylene isomers are predominantly separated through simulated moving bed (SMB) processes, which are adsorption-based processes operating at high temperature (~180 °C) and pressure (~9 bar).[1,2] Typical sorbents for these processes are cation-exchange faujasite zeolites that exhibit excellent thermal and chemical stability, but have low xylene saturation capacity (0.8–1.8 mmol g^{-1}) and *p*-xylene (PX) selectivity (smaller than 6).[1,3] New adsorbent candidates with either higher xylene uptake capacity or sorption selectivity have the potential to enable next-generation SMB.

Metal–organic frameworks (MOFs) or porous coordination polymers (PCPs), a family of inorganic–organic hybrid materials constructed from inorganic clusters and organic linkers *via* coordination bonds, have garnered tremendous interest in the field of chemical separations because of the rich engineering toolbox for tailoring the functionality, dimension, and geometry of pores.[4–11] Although efforts have been devoted to exploiting differences in thermodynamic interactions between MOFs and xylenes isomers to enable their separation,[12–15] high selectivities (>10) remain elusive.[7] Recently, MOF framework flexibility has been utilized to separate xylene isomers.[16–18] Lee *et al.* reported the breathing-assisted selective adsorption of PX in the pillar-bilayered MOFs [Zn_2(aip)$_2$(pillar)] [aip = 5-aminoisophthalic acid; pillar = 4,4′-bipyridine or 1,2-bis(4-pyridyl)ethane].[19] Shivanna *et al.* showed that selective PX adsorption is affected by the rotational barrier of the pyrazine pillars in Hofmann-type PCPs, which are coordination-dependent.[20] Yang *et al.* reported that flexible MOFs α-[Cu_2(pypz)$_2$] and β-[Cu_2(pypz)$_2$] [Hpypz = 4-(1*H*-pyrazol-4-yl)pyridine] selectively adsorb PX over *m*-xylene (MX) and *o*-xylene (OX) through a transformation to another phase [Cu_2(pypz)$_2$]· 0.5PX.[21] Nevertheless, it is difficult to predict the framework dynamics and xylene sorption properties prior to experimental measurements, which impedes rational design and rapid development of this class of materials.

Molecular sieving of PX has been realized in MOFs with tailored pore apertures as PX is somewhat smaller than the other C8 isomers (Scheme S1, ESI†). Nevertheless, most of these MOFs exhibit PX selectivities lower than 10,[7] which are underwhelming compared to the selectivities commonly seen in other chemical separation systems based on molecular sieving.[22–24] These moderate xylene selectivities could be attributed to the undesired flexibility of MOFs.[25,26]

Molecular sieving of xylene isomers may be realized by utilizing a rigid framework with minimal flexibility. One strategy to mitigate the effects of framework flexibility is constructing MOFs from rigid multidentate linkers. Linker rigidity reduces the possibility of linker bending and rotation, while increased linker connectivity helps confine linker translations in frameworks. Recently, purine derivatives have been employed as rigid ligands in MOFs for high-performance chemical separation,[27,28] but MOFs constructed with purine have not been studied for separation applications. Kahr *et al.* reported a series of MOFs that are constructed with purine building blocks.[29] Upon evaluating the single crystal structure

[a] *School of Chemical & Biomolecular Engineering, Georgia Institute of Technology, 311 Ferst Drive NW, Atlanta, GA 30332, USA. E-mail: ryan.lively@chbe.gatech.edu*
[b] *Department of Chemical Engineering, University of Florida, Gainesville, FL 32611, USA*
[c] *ChemMatCARS Beamline, The University of Chicago, Advanced Photon Source, Lemont, Illinois 60439, USA*
[d] *Oak Ridge National Laboratory, Oak Ridge, TN 37830, USA*
[e] *Lawrence Livermore National Laboratory, 7000 East Avenue, Livermore, CA 94550, USA*

† Electronic supplementary information (ESI) available. CCDC 2079261 and 2079262. For ESI and crystallographic data in CIF or other electronic format see DOI: https://doi.org/10.1039/d2cc04387d

‡ R. L. and Y. W. contributed equally to this work.

of this MOF family, we hypothesized that guest-free Zn(purine)X (X = OAc^-, Br^-) should be attractive adsorbent candidates for kinetic separations and even molecular sieving[22] of xylene isomers as it has a pore aperture of ~6 Å which lies within the target range.[7,30] Unfortunately, these materials were found to be nonporous, which is likely due to the blockage of pores by solvents or residual ligands.

Here, we report the synthesis and structural information of porous Zn(purine)X MOFs (X = I^- and Br^-). The gas sorption properties of these isostructural MOFs are reported for the first time, and Zn(purine)I exhibits excellent PX/OX ideal pseudo-equilibrium adsorption and diffusion selectivities of 16 and 6 at 303 K, respectively. The PX sorption selectivity of Zn(purine)I over OX under coadsorption scenarios is one of the best for xylene separation in MOFs to date.[7]

In the previous report, 2-nitroimidazole was used for the MOF synthesis, but it was not present in Zn(purine)X (X = OAc^- and Br^-).[29] Therefore, a modified synthetic method without 2-nitroimidazole was used for the synthesis of Zn(purine)X (X = I^- and Br^-) (ESI†). The powder X-ray diffraction (PXRD) pattern of Zn(purine)Br corresponds well to the literature as shown in Fig. 1. In addition, the similar XRD patterns of Zn(purine)Br and Zn(purine)I suggest that these MOFs share similar crystallographic structures. Attempts to synthesize Zn(purine)OAc *via* the modified synthesis method in the absence of 2-nitroimidazole were unsuccessful and produced an amorphous material.

Thermogravimetric analysis (TGA) and differential thermal analysis (DTA) profiles of Zn(purine)X (X = I^- and Br^-) were recorded to identify conditions of activating these MOFs for further characterization (Fig. S1, ESI†). The weight loss steps at ~200 °C can be attributed to the removal of solvents trapped in the frameworks. Heat activation at 200 °C appears to be sufficient for removing these solvent molecules as these weight loss steps disappear in the TGA and DTA curves of both activated materials (Fig. S2, ESI†).

Single-crystal X-ray diffraction (SCXRD) studies of activated Zn(purine)I and Zn(purine)Br crystals (Fig. S3, ESI†) suggest that both MOFs share the same RHO net topology (Fig. 1b–e and Table S1, ESI†). The Zn centers are tetrahedrally coordinated to two purine linkers *via* N-atoms from two different imidazole groups and a third purine linker *via* the pyrimidine N. Halide ligands occupy the last coordination sites of Zn coordination spheres, blocking the channels along *c* direction. Two types of channels with different openings lie alternatively along *b* direction (Fig. 1d and e), but only the larger channels are accessible to guest molecules (Fig. 2a, b and Fig. S4, ESI†). The calculated pore limiting diameters for the larger channels of Zn(purine)Br and Zn(purine)I are 5.6 Å and 5.5 Å, respectively.[31]

Ar adsorption experiments at 87.3 K revealed the porous nature of both MOF materials after activation (Fig. 2c and d). The BET surface areas of Zn(purine)Br and Zn(purine)I were calculated to be 142 and 130 $m^2\ g^{-1}$, respectively. These values are lower than the geometrically calculated accessible surface areas of Zn(purine)Br (391 $m^2\ g^{-1}$) and Zn(purine)I (329 $m^2\ g^{-1}$) using a probe radius of 1.7 Å (the van der Waals radius of Ar).

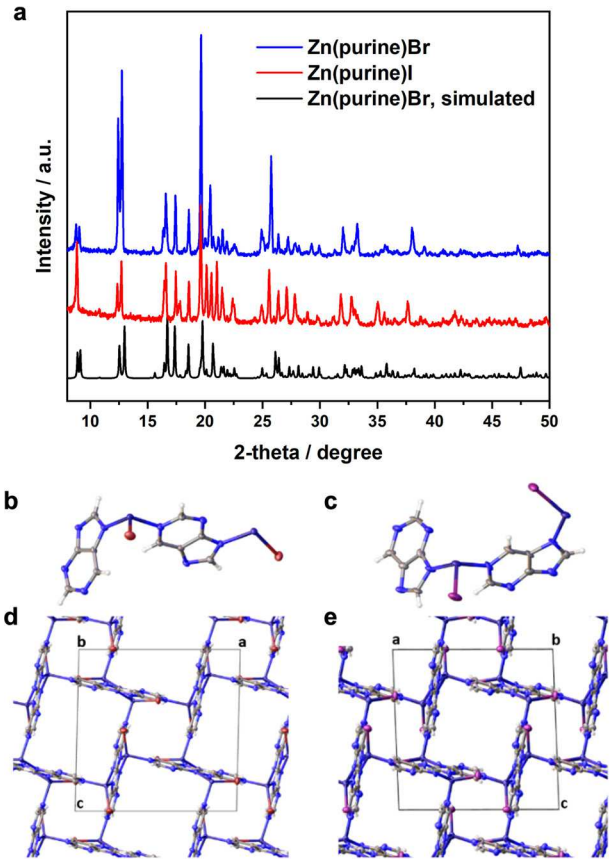

Fig. 1 (a) Experimental PXRD patterns of as-synthesized Zn(purine)Br and Zn(purine)I and the simulated PXRD pattern of unactivated Zn(purine)Br.[29] (b and c) The asymmetric unit obtained from SCXRD data of (b) Zn(purine)Br and (c) Zn(purine)I. (d and e) The packed structures view down the *b*-axis of (d) Zn(purine)Br and (e) Zn(purine)I. The difference in asymmetric unit appearance results from the different centering of their unit cells. C, grey; H, white; N, blue; Zn, dark blue; I, purple; Br, red.

Considering that the calculated binding energy of $CHCl_3$ is 0.268 eV per molecule (25.8 kJ mol^{-1}, Fig. S5, ESI†), $CHCl_3$ guest molecules should have been removed during the activation step. The lower than expected surface areas of the MOFs suggest that the reduced porosity might be the result of strongly-bound guest molecules that could not be replaced by $CHCl_3$.[32] Despite having low surface areas, Zn(purine)Br and Zn(purine)I exhibited moderate CO_2 uptake capacities of 2.0 mmol g^{-1} and 1.8 mmol g^{-1} at 1 bar at 298 K, respectively (Fig. S7, ESI†).

The small pore aperture of ~5.6 Å and rigid frameworks based on crystallographic measurements suggested that these MOFs may be promising molecular sieving materials for PX and OX isomers with kinetic diameters of 5.8 Å and 6.8 Å, respectively.[33] Single-component xylene vapor adsorption studies were conducted to evaluate the xylene sorption properties of these MOFs. No xylene adsorption in Zn(purine)Br was observed. However, Zn(purine)I exhibited PX and OX uptake capacities of 1.9 wt% (0.18 mmol g^{-1}) and 0.1 wt% with a 0.05 xylene vapor activity at 303 K, respectively, corresponding to an approximate guest occupancy of 0.44 PX molecules and 0.023 OX molecules per unit cell. Accordingly, the pseudo-equilibrium

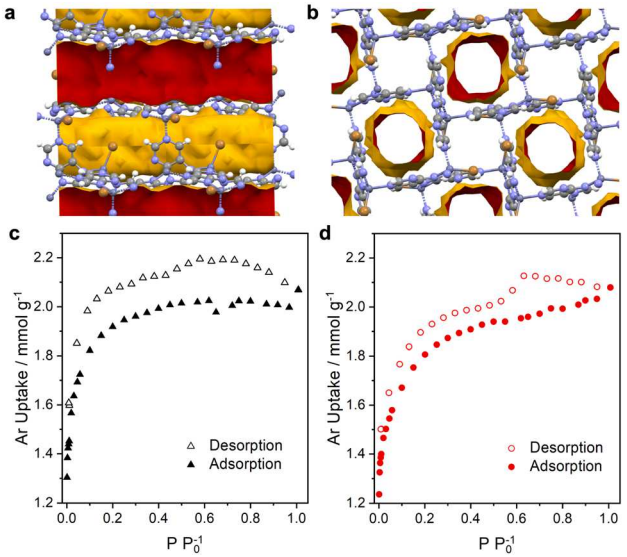

Fig. 2 (a and b) Pore shape and accessible volumes indicated by yellow surfaces of Zn(purine)Br viewed along the (a) *b*- and (b) *a*-axis using a probe radius of 1.2 Å (red surfaces represent the cross-section of the pores). Continuous 1D channels can be seen along the *b*-axis allowing the passage of guest molecules. C, grey; N, blue; Zn, dark grey; H, white; Br, orange. (c and d) Ar adsorption (closed symbols) and desorption (open symbols) isotherms of (c) Zn(purine)Br and (d) Zn(purine)I at 87.3 K for BET surface area determination.

ideal sorption capacity ratio of PX and OX is about 16, which is greater than that (3–5) of faujasite-type zeolites used in industrial SMB processes.[2] The high selectivity of PX over OX exhibited in Zn(purine)I coupled with the low overall uptake is consistent with the conclusions drawn in a recent computational prediction of xylene separation that high PX selectivity is typically accompanied with low PX uptake capacity.[30] In addition, the similar PXRD patterns of Zn(purine)I powder loaded with xylene vapors (Fig. S8, ESI†) suggested no signs of phase transition triggered by the presence of xylene guests in the framework.

The transport diffusivities of PX and OX in Zn(purine)I were obtained *via* fitting the kinetic adsorption curve with a Fickian diffusion model (Fig. 3a). The assumption of the diffusion path along the *b*-axis, which corresponds to the longest dimension of the crystals, was determined using the Mercury software (Fig. S9, ESI†). Particle size distribution of Zn(purine)I (Fig. S10 and Table S3, ESI†) was calculated by ImageJ, and details of the calculation are described in the (ESI†). At 303 K and 0.05 vapor activity, the PX and OX transport diffusivities are 4.5×10^{-12} cm^2 s^{-1} and 0.8×10^{-12} cm^2 s^{-1}, respectively. This results in a PX/OX diffusion selectivity of 6. Kinetic selectivities of this magnitude are rarely observed in MOFs.[15,31] Self-diffusion in Zn(purine)I by pulsed field gradient – nuclear magnetic resonance (PFG-NMR) spectroscopy revealed a diffusivity of 8×10^{-10} cm^2 s^{-1} for PX at a similar temperature of 296 K (Fig. S11, ESI†). However, this can mostly be due to the much smaller length scale of diffusion observation (300 nm) in PFG-NMR than in the macroscopic kinetic adsorption measurements. OX diffusion could not be measured by PFG-NMR due to signal-to-noise limitations.

Liquid phase batch adsorption experiments of PX and OX mixtures were performed to examine the xylene separation performance of Zn(purine)I. 1,3,5-Triisopropylbenzene (TIPB) with a kinetic diameter of 8.5 Å[34] was selected over typically used linear alkanes as the diluting bulky solvent to avoid solvent adsorption during the sorption experiments, and the even bulkier 1,3,5-tri-*tert*-butylbenzene (TTBB) was selected as an internal non-adsorbed marker.[19] As shown in Fig. 3b, the PX concentration in the liquid phase decreased from the beginning of the experiment and stabilized at around 0.085 M after 1 day, indicating adsorption of PX into Zn(purine)I. Mass balance calculation estimates that the PX uptake capacity of Zn(purine)I was about 0.51 mmol g^{-1} at an activity of 0.02 at 298 K. In contrast, the liquid phase concentration of OX did not appreciably change during the adsorption experiment, suggesting that negligible amount of OX was adsorbed by Zn(purine)I within 7 h. In addition, Zn(purine)I selectively adsorbed PX from an equimolar ternary mixture of PX/OX/MX but excluded MX and OX (Fig. 3c), and the PX uptake was as high as 0.54 mmol g^{-1} at an activity of 0.02 at 298 K. These experiments suggest that xylene sorption selectivities in Zn(purine)I are

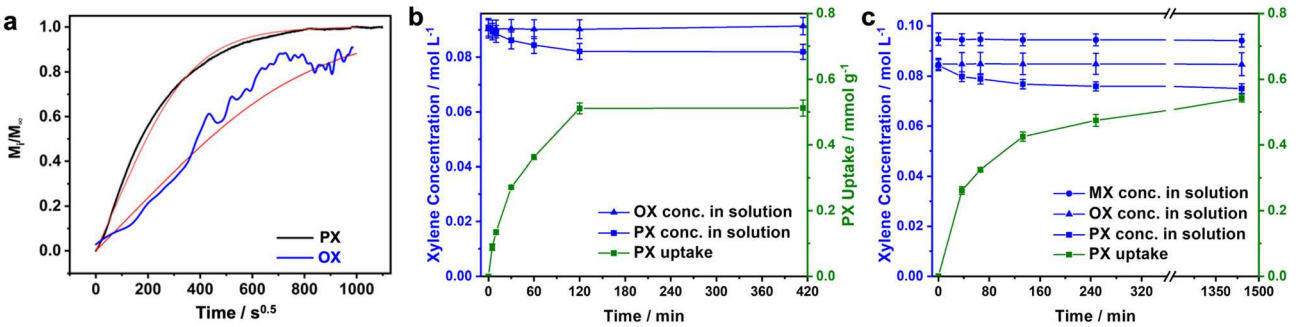

Fig. 3 (a) Kinetic uptake curves of PX (black) and OX (blue) in Zn(purine)I and the curve fittings to determine transport diffusivities (red). For clarity, the OX experimental data were smoothed using an FFT Filter Method with 40 points of window. (b) Time-dependent liquid-phase concentrations of xylene isomers (PX and OX) and PX uptakes in Zn(purine)I in coadsorption experiments in TIPB at room temperature. Initial concentrations of PX and OX were both 0.09 M. (c) Time-dependent liquid-phase concentrations ternary xylene isomer system (PX, MX, and OX) and PX uptakes in Zn(purine)I in coadsorption experiments in TIPB at room temperature.

dependent on the differences in xylene dimensions, and that only PX with the slimmest profile can be adsorbed. In comparison, UiO-66, a Zr MOF with a comparable pore window size (5.6 Å) but freely rotatable phenyl rings and larger cavities, did not exhibit noticeable selectivity towards any of xylene isomers as indicated by their comparable uptakes (Fig. S12, ESI†), highlighting the critical roles of combining suitable pore apertures and framework rigidity in realizing highly selective molecular sieving of xylene isomers in MOFs (Table S4, ESI†). Further analyses of the similar PXRD patterns of Zn(purine)I before and after liquid-phase xylene adsorption experiments confirm the excellent stability of Zn(purine)I (Fig. S13, ESI†).

In summary, we have successfully demonstrated the preparation of porous purine Zn MOF Zn(purine)Br and its isostructural variant Zn(purine)I. The synthesis procedure was optimized from a previously reported method to prevent pore blockage. Zn(purine)I features a high PX/OX diffusion and adsorption selectivity owing to small channel sizes and rigid framework, which along with its excellent thermal stability makes it a promising candidate for xylene isomer separation. Future development to improve the MOF's kinetic properties could make it highly attractive for next-generation SMB separations.

This work was performed with support from the Center for Understanding and Control of Acid Gas-Induced Evolution of Materials for Energy (UNCAGE-ME), an Energy Frontier Research Center funded by the U.S. Department of Energy, Office of Science, Office of Basic Energy Sciences, under award no. DE-SC0012577.

ChemMatCARS Sector 15 is supported by the National Science Foundation under grant number NSF/CHE-1834750. This research used resources of the Advanced Photon Source, a U.S. Department of Energy (DOE) Office of Science User Facility operated for the DOE Office of Science by Argonne National Laboratory under Contract No. DE-AC02-06CH11357.

Conflicts of interest

The authors declare no competing financial interests.

Notes and references

1 M. P. M. Nicolau, P. S. Bárcia, J. M. Gallegos, J. A. C. Silva, A. E. Rodrigues and B. Chen, *J. Phys. Chem. C*, 2009, **113**, 13173–13179.
2 Q. Shi, J. C. Gonçalves, A. F. P. Ferreira and A. E. Rodrigues, *Chem. Eng. Process.*, 2021, **169**, 108603.
3 M. Minceva and A. E. Rodrigues, *Chem. Eng. Res. Des.*, 2004, **82**, 667–681.
4 M. Ding, R. W. Flaig, H.-L. Jiang and O. M. Yaghi, *Chem. Soc. Rev.*, 2019, **48**, 2783–2828.
5 B. R. Barnett, M. I. Gonzalez and J. R. Long, *Trends Chem.*, 2019, **1**, 159–171.
6 S. Mukherjee and M. J. Zaworotko, *Trends Chem.*, 2020, **2**, 506–518.
7 Z. Zhang, S. B. Peh, C. Kang, K. Chai and D. Zhao, *EnergyChem*, 2021, **3**, 100057.
8 Z. R. Herm, E. D. Bloch and J. R. Long, *Chem. Mater.*, 2014, **26**, 323–338.
9 V. Finsy, H. Verelst, L. Alaerts, D. De Vos, P. A. Jacobs, G. V. Baron and J. F. M. Denayer, *J. Am. Chem. Soc.*, 2008, **130**, 7110–7118.
10 L. Alaerts, C. E. A. Kirschhock, M. Maes, M. A. van der Veen, V. Finsy, A. Depla, J. A. Martens, G. V. Baron, P. A. Jacobs, J. F. M. Denayer and D. E. De Vos, *Angew. Chem., Int. Ed.*, 2007, **46**, 4293–4297.
11 D. M. Polyukhov, A. S. Poryvaev, A. S. Sukhikh, S. A. Gromilov and M. V. Fedin, *ACS Appl. Mater. Interfaces*, 2021, **13**, 40830–40836.
12 M. I. Gonzalez, M. T. Kapelewski, E. D. Bloch, P. J. Milner, D. A. Reed, M. R. Hudson, J. A. Mason, G. Barin, C. M. Brown and J. R. Long, *J. Am. Chem. Soc.*, 2018, **140**, 3412–3422.
13 S.-I. Kim, S. Lee, Y. G. Chung and Y.-S. Bae, *ACS Appl. Mater. Interfaces*, 2019, **11**, 31227–31236.
14 X. Li, J. Wang, N. Bai, X. Zhang, X. Han, I. da Silva, C. G. Morris, S. Xu, D. M. Wilary, Y. Sun, Y. Cheng, C. A. Murray, C. C. Tang, M. D. Frogley, G. Cinque, T. Lowe, H. Zhang, A. J. Ramirez-Cuesta, K. M. Thomas, L. W. Bolton, S. Yang and M. Schröder, *Nat. Commun.*, 2020, **11**, 4280.
15 F. Vermoortele, M. Maes, P. Z. Moghadam, M. J. Lennox, F. Ragon, M. Boulhout, S. Biswas, K. G. M. Laurier, I. Beurroies, R. Denoyel, M. Roeffaers, N. Stock, T. Düren, C. Serre and D. E. De Vos, *J. Am. Chem. Soc.*, 2011, **133**, 18526–18529.
16 V. Finsy, C. E. A. Kirschhock, G. Vedts, M. Maes, L. Alaerts, D. E. De Vos, G. V. Baron and J. F. M. Denayer, *Chem. – Eur. J.*, 2009, **15**, 7724–7731.
17 S. Mukherjee, B. Joarder, B. Manna, A. V. Desai, A. K. Chaudhari and S. K. Ghosh, *Sci. Rep.*, 2014, **4**, 5761.
18 Y. Yang, P. Bai and X. Guo, *Ind. Eng. Chem. Res.*, 2017, **56**, 14725–14753.
19 J. Lee, Y. Kim, Y. Son, H. Kim, Y. Nam Choi, D. D'Alessandro, P. Chandra Rao and M. Yoon, *Chem. – Eur. J.*, 2021, **27**, 14851–14857.
20 M. Shivanna, K.-i Otake, J.-J. Zheng, S. Sakaki and S. Kitagawa, *Chem. Commun.*, 2020, **56**, 9632–9635.
21 X. Yang, H.-L. Zhou, C.-T. He, Z.-W. Mo, J.-W. Ye, X.-M. Chen and J.-P. Zhang, *Research*, 2019, **2019**, 9463719.
22 Y. Wang and D. Zhao, *Cryst. Growth Des.*, 2017, **17**, 2291–2308.
23 H. Wang, Y. Liu and J. Li, *Adv. Mater.*, 2020, **32**, 2002603.
24 A. Cadiau, K. Adil, P. M. Bhatt, Y. Belmabkhout and M. Eddaoudi, *Science*, 2016, **353**, 137–140.
25 J. H. Lee, S. Jeoung, Y. G. Chung and H. R. Moon, *Coord. Chem. Rev.*, 2019, **389**, 161–188.
26 C. Gu, N. Hosono, J.-J. Zheng, Y. Sato, S. Kusaka, S. Sakaki and S. Kitagawa, *Science*, 2019, **363**, 387–391.
27 Z. Zhang, S. B. Peh, Y. Wang, C. Kang, W. Fan and D. Zhao, *Angew. Chem., Int. Ed.*, 2020, **59**, 18927–18932.
28 R. K. Gupta, M. Riaz, M. Ashafaq, Z.-Y. Gao, R. S. Varma, D.-C. Li, P. Cui, C.-H. Tung and D. Sun, *Coord. Chem. Rev.*, 2022, **464**, 214558.
29 J. Kahr, J. P. S. Mowat, A. M. Z. Slawin, R. E. Morris, D. Fairen-Jimenez and P. A. Wright, *Chem. Commun.*, 2012, **48**, 6690–6692.
30 Z. Qiao, Y. Yan, Y. Tang, H. Liang and J. Jiang, *J. Phys. Chem. C*, 2021, **125**, 7839–7848.
31 T. F. Willems, C. H. Rycroft, M. Kazi, J. C. Meza and M. Haranczyk, *Microporous Mesoporous Mater.*, 2012, **149**, 134–141.
32 Y. G. Chung, J. Camp, M. Haranczyk, B. J. Sikora, W. Bury, V. Krungleviciute, T. Yildirim, O. K. Farha, D. S. Sholl and R. Q. Snurr, *Chem. Mater.*, 2014, **26**, 6185–6192.
33 R. Szostak, *Handbook of Molecular Sieves*, Van Nostrand Reinhold, New York, 1992.
34 L. T. Canham and A. J. Groszek, *J. Appl. Phys.*, 1992, **72**, 1558–1565.

